INSTRUMENTATION HIGHLIGHTS AT LEP

GERT M. VIERTEL
EIDGENÖSSISCHE TECHNISCHE HOCHSCHULE
INSTITUT FÜR HOCHENERGIEPHYSIK
ZÜRICH, SWITZERLAND

INTRODUCTION

The large electron positron storage ring (LEP) at CERN will come into operation at the end of 1988. The four collaborations (Aleph, Delphi, L3 and Opal), approved in 1983, have done an enormous effort in prototyping their most ambitious components to prove their feasibility. Since most of the detector components are larger than ever built, time is getting short, even 4 years ahead of the setting-up schedule. This report gives a brief description and presents the status of 4 out of about 50 detector components (a choice which was not easy to make):

- Time Projection Chamber (TPC) in Aleph
- High Density Projection Chamber (HPC) in Delphi
- Bismuth Germanate ($Bi_4Ge_3O_{12}$: BGO) in L3
- Jet Chamber in Opal

TPC (ALEPH)

As central detector, a Time Projection Chamber was chosen to aim at good momentum and angular resolution and ease in pattern recognition. In a cylindrical active volume of 2 x 2.2 m length and an inner and outer radius of 33 cm and 177 cm respectively, points along the charged particle tracks are measured in three dimensions at the endplates of the TPC by a system of proportional wires and readout pads. In addition dE/dx is determined from 320 pulse height samples per track on the proportional wires. A total of 50'000 electronics channels are planned. To study electric and magnetic field inhomogenities, space charge effects (gating grid plane), electron attachment, mechanical construction, choice of materials and other problems, a full size sector including magnet (so called TPC 90) was built and is currently under test by means of a laser system and cosmic rays. The reconstructed laser track points have been found to deviate from straight tracks by less than 50 μm (Fig. 1, no corrections applied). The r-Φ resolution obtained is 180 -240 μm. Fig. 2 shows the response function of the 8 mm long pads, Fig. 3 **shows its dependence on** the magnetic field for two different drift lengths. From preliminary measurements a double track resolution of about 1 cm is deduced. References: A. Peisert, CERN EP Seminar (1984)/W. Blum, private communication/Technical proposal Aleph, LEPC 83-2 (1983) / CERN, LEPC 84-10 (1984).

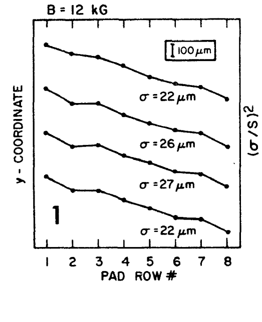

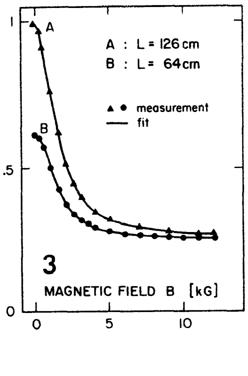

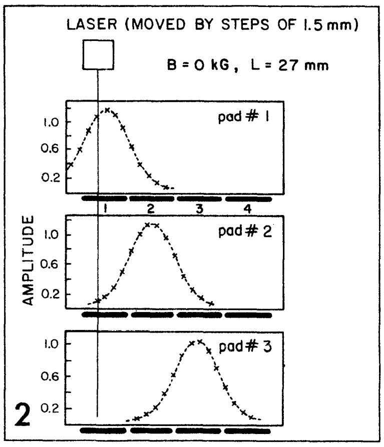

HPC (DELPHI)

Electromagnetic showers as well as charged hadrons are detected in the HPC, a novel instrument, which allows charge measurements in volume elements with a resolution only limited by the number of electronics readout channels foreseen. The detector planned has a total lead absorber thickness of 20 X_0, a length of 520 cm, a total weight of 100 tons and is subdivided into 160 submodules. Each module consists of converter planes perpendicular to the particle entrance direction interleaved by ten mm wide gaps, where the ionization charge drifts up to 65 cm in a uniform electric field towards the detection plane of proportional chambers with a cathode pad structure. To this bidimensional information the third coordinate is added by measuring the drift time of the charge buckets. Finite element calculations were performed to study the deformation of the converter structure, produced by an interesting lead wire ribbon technique, on its stiffening bars. A full size prototype is currently under construction. First results of measurements on a small test set-up are shown in Fig. 4 (angular resolution of showers) and Fig. 5 (energy resolution as a function of electron energy with magnet fields parallel to the drift field). References: A. Berggren at al., CERN-EF 83-13 (1983)/A. Berggren et al., Delphi HPC Calorimeter (1984)/Technical Report Delphi, CERN LEPC 83-3 (1983)/ H.G. Fischer, Novosibirsk Conference (1984)/ A. Ullaland, private communication.

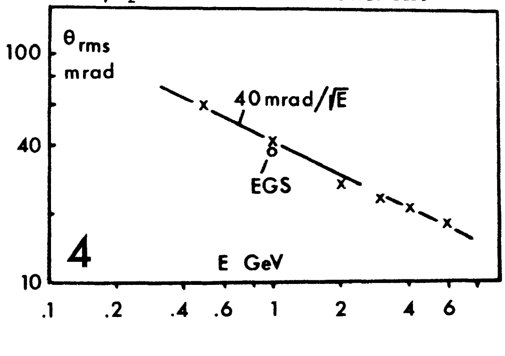

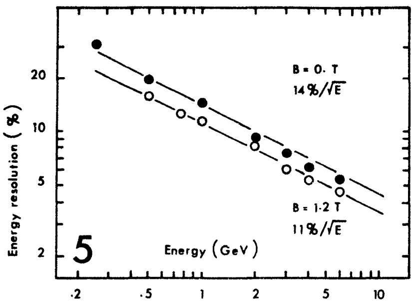

BGO (L3)

The electromagnetic calorimeter will consist of 12'000 tapered BGO crystals with a front area of ~ 2x2 cm^2 all pointing to the interaction region. The table summarizes the properties of bismuth germanate:

	$Bi_4Ge_3O_{12}$	NaI (Tl)	BaF_2	$CdWO_4$
DENSITY [g/cm^3]	7.13	3.67	4.9	7.9
RADIATION LENGTH [cm]	1.12	2.59	2.1	
MAXIMUM EMISSION [Å]	4800	4100	2250/3100	5400
DECAY CONSTANT [ns]	300	230	0.6 / 620	5000
AFTERGLOW (@ 3ms) [%]	0.005	0.5 - 5.0		0.005
HYGROSCOPIC	NO	YES	NO	NO
INDEX OF REFRACTION	2.15	1.85	1.56	2.3
RELATIVE LIGHT OUTPUT	10-14	100	5/16	38
TEMPERATURE COEFFICIENT OF LIGHT OUTPUT [% / °C]	-1.7	0.22—0.9		0
NUCLEAR ABSORPTION LENGTH [cm]	23			
MOLIERE RADIUS [cm]	2.24			
CRITICAL ENERGY [MeV]	10.5			
dE / dx [MeV/cm]	8			

BGO allows the reduction of the detector volume by a factor of three compared to NaI (Tl) and has the advantage of being non-hygroscopic. The light yield is low but sufficient for a photodiode (HAM S-1790) readout, which is mandatory because of the 5 kGauss detector environment. Because of the high temperature coefficient of the light output, each crystal will be equipped with a thermal sensor to allow for regulation of the temperature within ± .1^{o}C.

The design goals of the calorimeter are:
- Energy resolution σ/E ~ 1% from 1 to 100 GeV
- Position resolution of a few mm
- Hadron rejection ≳ 1000
- Shower separation inside jets.

Tests done focussed on linearity (Fig.6) energy resolution (Fig.7), crystal surface influence on uniformity (Fig.8), position resolution (Fig.9), and studies of radiation damage:
- Damage by photons and particles causes changes of BGO's absorption properties
- Damage is not linear with dose (saturation effects observed above 1000 Rad)
- Damage depends on crystal quality (impurities)
- Damaged BGO spontaneously recovers (Fig.10) with 3 time constants:
  T1 ~ 1h, T2 ~ 1d, T3 ~ 1 month
- Temperature speeds up recovering.
- Damage in NaI(Tl) is similar to BGO

References: M. Schneegans, San Miniato conference, Florence (1984)/G.J. Bobbink et al., Carnegie-Mellon (1984)/C. Laviron et al., CERN EF 84-05 (1984)/Technical Report L3, LEPC 83-5 (1983).

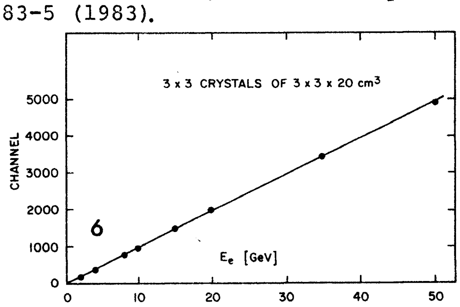

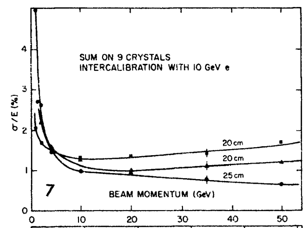

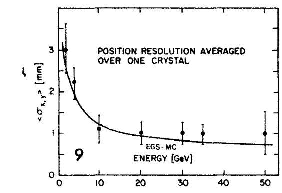

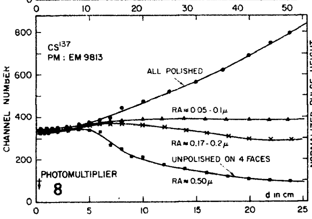

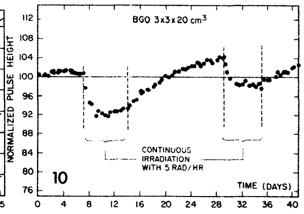

JET CHAMBER (OPAL)

The central tracking detector inside a 4 kGauss solenoid consists of three parts: a small vertex chamber around the beam pipe, a special chamber at a radial distance of 185 cm from the beam pipe for a precise measurement of the Z coordinate, and in between a large jet chamber (similar to the chamber built for Jade at Desy, successfully running for several years). In 24 segments a total of 3840 sense wires, equipped with Flash-ADC's on both ends, and 19800 field wires will be mounted between two conical aluminium end plates at a distance of ~ 4m. Two full size segments are currently under construction, since prototyping proved that the design goals could be reached (test result):
- mechanical tolerances on the sense wire position: 50μm(10μm)
- Resolution σ(RΦ) at 4 bars: 150μm(120μm/ Fig. 11)
- Systematic error on the sagitta: 50μm (~30μm/Fig.12)
- Resolution σ(Z) : 0.6-1.0% (~1.0%/Fig.13)
- Double track resolution: 3 mm(2.5-3.0 mm)
- Resolution σ(dE/dx) : 3.5% (3.6%/160 samples). References: Technical Report Opal, LEPC 83-4 (1983)/R.D. Heuer, SLAC Workshop (1983).

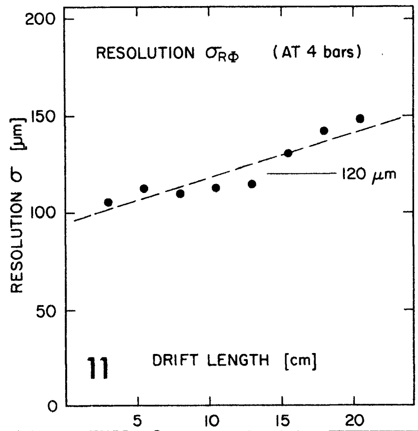

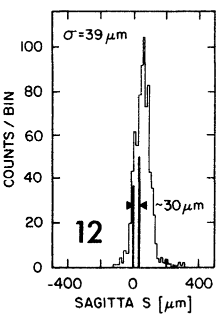

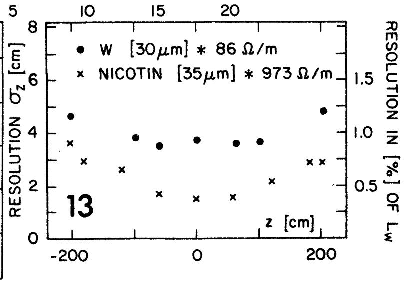

MICROSTRIP DETECTORS

Rudolf Leiste

Institut für Hochenergiephysik
der Akademie der Wissenschaften der DDR
Berlin-Zeuthen, GDR

I. INTRODUCTION

Semiconductor devices as particle detectors in nuclear spectroscopy are known since more than 25 years. Use in high energy physics started as pure silicon became available, the introduction of the planar process opened the possibility for industrial production (suppliers in Europe and USA) of microstrip detectors with reproducible parameters and strip pitches down to 20 μm. Typically 10-20 planes with 500-1000 strips/plane are used at present in about 10 experiments on heavy flavour search at CERN and FNAL, there are plans to use several hundred planes in LEP experiments.

II. WORKING PRINCIPLE AND FABRICATION

In silicon, about 80 free electron-hole pairs/μm are produced by a minimum ionizing particle. Their mobility is sufficiently high ($v/E=1350$ cm^2/V·s for electrons), the minority charge carrier lifetime can be of the order of milliseconds. Rectifying structures provide a low dark current at high electric field inside the semiconductor for fast charge collection. The p-n-junctions are produced in a planar process (ion implantation plus oxide passivation, fig.1), starting usually from n-type silicon wafers, orientation $\langle 111 \rangle$, diameter 2-4'', thickness $D=300$-1000 μm, resistivity $\varrho=1$-20 kΩ·cm.

Advantages: 1) silicon is working at 300°K, 2) oxide passivation protects against ambient conditions, 3) complicated structures possible, 4) well suited for industrial production. Drawbacks: 1) dense material (300 μm Si $\hat{=}$ .03X_0), 2) radiation damage, 3) limited size of single detectors, 4) needs industry.

III. PERFORMANCE

A. Technical parameters

- Depletion depth $d=.53\sqrt{\varrho \cdot U} = 300$ μm for $\varrho = 3$ kΩ·cm at 110 V.
- Leakage current $i_{leak} \sim U^x$, depends on fabrication, 100-300pA reached for strips 50 μm·5cm, $i_{leak} \lesssim 10$nA/strip practically does not affect the total noise.
- Breakdown voltage $U_{max}=f$ (fabrication)$>U_D$
- Charge collection time typically 10 ns.

B. Applicative parameters

- Signal-to-noise ratio = f (amplifier, i_{leak}, C_{in}), $\langle S \rangle / \sigma_N = 10$-$20$ (fig.2), i.e. $\sigma_N = 1000$-2000 e^-
- Efficiency and number of spurious hits are directly related to $\langle S \rangle / \sigma_N$ (fig.3)

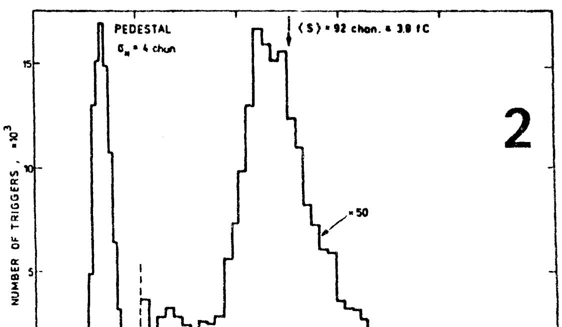

- Internal crosstalk (passage of the interstrip region, charge diffusion) is negligible at least down to 50 μm pitch (fig.4)
- Dead zones between strips are very small, if any.

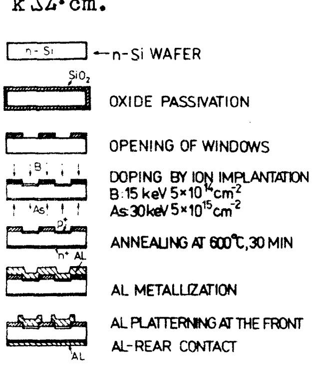

1

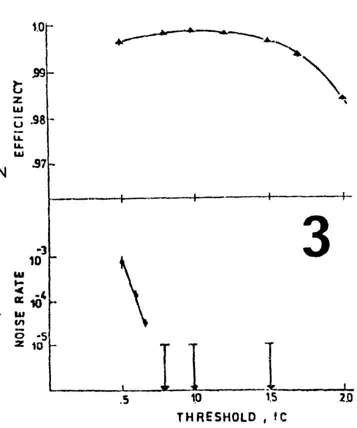

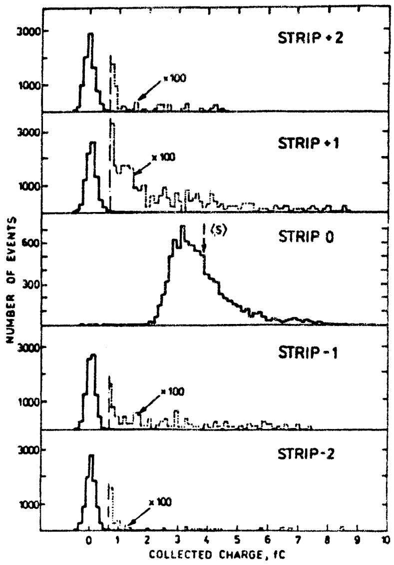

4

IV. READOUT SCHEMES strongly influence the accuracy σ_x and double track resolution δ_2.

A. Digital readout

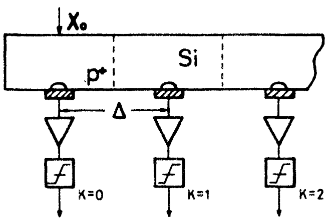

$X = X_0 + K\cdot\Delta$
$\sigma_x \cong \Delta/\sqrt{12}$
$\delta_2 \cong 2\Delta$
+ : Fast triggering
— : $N_{CHANNEL} = N_{STRIPS}$

Technical limitations, only for small systems.

B. Analog readout with charge division

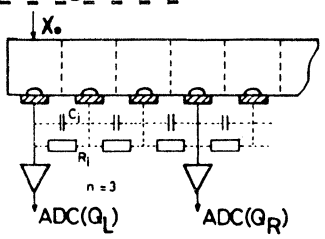

$X = X_0 + n\cdot\Delta\cdot Q_R/(Q_L + Q_R)$
+ : $\sigma_x = 4.5\,\mu m_{(n=3,\Delta=20\mu m)} \leq \Delta/\sqrt{12}$
— : $\delta_2 \cong n\cdot\Delta$
+ : $N_{CHANNEL} = N_{STRIPS}/n$
— : No fast triggering

Charge diffusion at $\Delta < 50\,\mu m$ improves σ_x, but limitations on n due to noise and crosstalk problems.

C. Silicon drift chamber (SDC)

New device proposed by Gatti and Rehak, under study. Preliminary: Drift over 8 mm without signal attenuation (MPI Munich).

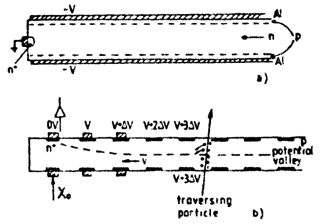

$X = X_0 + v\cdot t$
$\sigma_x = ?$
$\delta_2 = ?$
+ : $N_{CHANNEL} \ll N_{STRIPS}$
— : No fast triggering

V. READOUT ELECTRONICS

General problems for the readout electronics are a) the very low signal ($\langle Q\rangle \approx 4$ fC) and b) the high number of channels (except for the SDC), which creates problems of stability, power dissipation, cost, and space needed close to the detector. Three solutions can be envisaged:

- A solution using standard components is possible, but only for small systems (~1000 channels).
- The hybrid solution is feasible for medium size systems in fix target experiments, a preamp is commercially available, a serialisation chip will be soon (fig.5).
- A fully integrated readout including serialisation seems the only possible solution for big systems expecially at colliders. The connection to the detector strips will be done by wire bonding, may be later by on-chip integration with the detectors. Two schemes are under development: i) the traditional scheme amplifier - intermediate storage - clocked serial readout (fig.6, MPI Munich/Univ. Dortmund, CERN/SLAC); ii) direct parallel coupling of the detector strips to a CCD (Univ. Delft). In both schemes there is no possibility for fast triggering (not important for collider experiments).

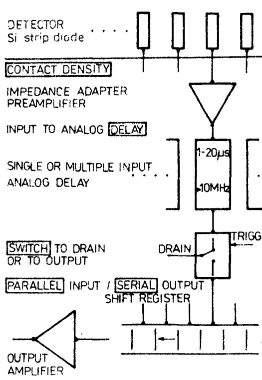

5

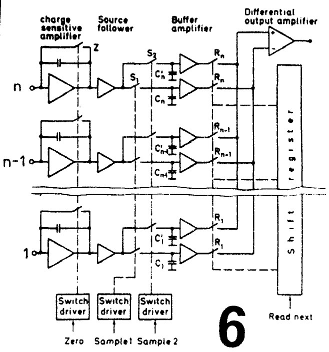

6

VI. CONCLUSIONS

i) No major open questions concerning detector fabrication.

ii) The detectors provide high accuracy ($\gtrsim 2\,\mu m$), high double track resolution and almost 100 % efficiency.

iii) Major drawbacks are the limited size, the relatively high density and the problems of radiation damage.

iv) The main problem now is the readout electronics, a solution may be expected in the next few years.

REFERENCES: III. Symposium on Semiconductor Detectors, Munich 1983, NIM, in press; G. Charpak, F. Sauli, CERN-EP/84-35; P.G. Rancoita, /NFN/AE-83/7; A.M. Walenta, Si-83-23; G. Bellini, L. Foà, M.A. Giorgi, Phys. Rep. 83/1(82)9.

RECENT RESULTS ON A COMPACT LEAD-SCINTILLATOR SHOWER COUNTER WITH PHOTODIODE READOUT*)

J. Ahme, J. Marks, H. Spitzer, K. Wittenburg (Universität Hamburg)
G.-G. Winter (DESY)
H. Greif, H. Oberlack (MPI für Physik München)

We have used silicon photodiodes in combination with wavelength shifters (w.l.s.) to read out lead-scintillator shower counters. Our objective is to build a compact electron tagging counter for the CELLO detector at PETRA and to develop calorimeter prototypes for experimentation at HERA. Although not amplifying the signal, photodiodes have the advantage of operating in strong magnetic fields with a very stable yield (to better than 1 %). By concentrating the scintillation light on a diode of small area via a wavelength shifter bar, acceptable signal to noise ratios can be obtained. Initial results proving the feasibility of such a scheme have been reported in ref. 1. In the meantime we have improved on the light yield considerably. Reported below are comparisons of the light yield from different scintillators and results obtained with a realistic module fitted to the geometry of the PETRA environment.

The light yields from different scintillator and wavelength shifter combinations were compared using a sandwich, with dimensions 50x50x300 mm^3, containing an average of 38 samplings of 2.5 mm lead and 4-6 mm thick scintillator sheets. The scintillator was read out via a 3x30x300 mm^3 w.l.s. bar connected to a 1 cm^2 silicon photodiode (Hamamatsu S1790) and a charge sensitive preamplifier (Canberra 2003 BT). The following table shows the materials tested and the relative light yields from electron showers (3 GeV) normalized to a constant scintillator thickness of 4 mm.

material	thickness	relative light yield per 4 mm scint.
Altustipe + BBQ	6	1
NE 104 B + BBQ	4	2.15
SCSN 38 + Y7	5	2.42

We observe the highest yield from the polystyrene scintillator SCSN 38 and the w.l.s. Y7 specially matched to it (ref. 2). A separate measurement was made using 43 samplings of 4 mm thick SCSN 38 scintillator and 2.5 mm thick lead sheets, yielding 14 500 photoelectrons per GeV of incoming electron energy.

Next we used the latter scintillator-w.l.s. combination in nine prototype-modules of the shape shown in fig. 1, which fit into the anticipated geometry on the PETRA beampipe. 46 samplings of 2.5 mm lead and 4 mm

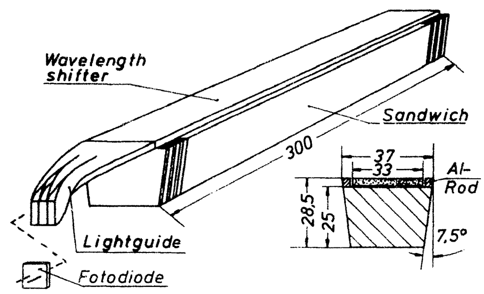

fig.1 Sandwich prototype (dimensions in mm)

scintillator, with an effective radiation length of 14 mm, were read out by a 1 cm^2 photodiode. For amplification and shaping (τ=2μsec) of the signal hybridized electronics built at the MPI München were used. We observed a yield of about 24 000 photoelectrons/GeV. The energy resolution was measured to be $\sigma_E/E=0.107/\sqrt{E}$ for energies from 1 to 6 GeV (see fig. 2). The combined noise from the diode and the preamplifier was about 800 e_0, corresponding to a noise equivalent energy of σ_{rms}=30 MeV. This gives a negligible contribution to the energy resolution for energies above 1 GeV.

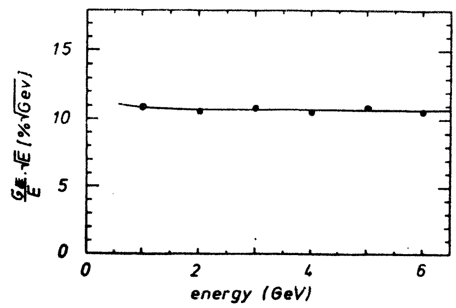

fig. 2

The improved light yield and noise performance compared to our results reported in ref. 1 is both due to the better scintillator-w.l.s. combination and to a better light concentration. The small transverse dimensions of the module allow a small shifter to cover a large solid angle. In addition the trapezoidal shape favors efficient light collection.

In summary, we have successfully used silicon photodiodes for the read out of compact electromagnetic scintillator calorimeter modules, yielding about 24 000 photoelectrons per GeV.

Ref.1: J. Ahme et al.,Nucl.Instr.Meth.221(1984)543
Ref.2: T. Kamon et al.,Nucl.Instr.Meth.213(1983)261

* presented by H. Spitzer, II. Institut für Experimentalphysik, D-2000 Hamburg 50, FRG.

SCINTILLATING GLASS FIBER-OPTIC IMAGING SYSTEM FOR TRACKING APPLICATIONS*

R. Ruchti, B. Baumbaugh, J. Bishop, N. Cason, S. Grenquist, V. Kenney, E. Mannel, R. Mountain, W. Shephard, and P. Wilkins
Department of Physics, University of Notre Dame, Notre Dame, IN 46556, USA
A. Kreymer
Fermi National Accelerator Laboratory, Batavia, IL 60510, USA
A. Rogers
Synergistic Detector Designs, Mountain View, CA 94043, USA
R. Mead and D. Swanson
Collimated Holes, Inc., Campbell, CA 95025, USA

ABSTRACT

Coherent, scintillating glass fiber-optic plates containing Terbium and Cerium Oxides have been developed to detect high energy particle interactions with high spatial resolution.

1. INTRODUCTION: We are developing devices which exploit the "local" fluorescence properties of trivalent Terbium and Cerium oxides in silicate glass compositions. These glasses constitute the core material of cladded-glass fibers which are formed into coherent fiber-optic plates. The combined features of "local" fluorescence and "total" internal reflection within the fibers allows the reconstruction of trajectories of ionizing particles produced in high energy reactions. The devices are suitable for both fixed target and colliding beam applications.

2. OPTICAL-IMAGING SYSTEM: The detector imaging system is shown in Fig. 1 and consists of an active detection element which is a scintillating fiber optic plate. The plates are typically 1 cm^3 in volume with constituent fibers of 10 μm - 25 μm in cross section. The volume fraction of active (core) glass is ~75%.

Details of the fluorescence properties of the scintillating glasses have been presented elsewhere[1]. For the Terbium glass, principal emission occurs at 550 nm with slow fluorescence decay $\tau \sim 3.5$ msec. For the Cerium glass, principal emission occurs at 395 nm with fast fluorescence decay $\tau \sim 40$ nsec. For our particular fiber optic plates the indices of refraction for core and clad are n = 1.58, n = 1.50 respectively. For these values, typically 10% of the produced scintillation light is trapped by total internal reflection within the fibers. Extramural absorber is incorporated on the outer surfaces of the cladding to suppress untrapped light.

The trapped light is presented to the input fiber-optic faceplate of a 3-stage image intensifier. Overall system luminescence gain is 2 x 10^5 which is sufficient for either film or electronic data recording using VIDICON or CCD systems. We are currently recording data using a contact-camera. Data film is held against the output fiber-optic plate of the image intensifier via vacuum pull-down, obviating the need for lenses.

Fig. 2 (a) shows an interaction of a ~600 GeV/c neutron in a Ce glass target comprised of 25 μm fibers of 0.8 cm length, and Fig. 2 (b) is a 10 GeV/c π^- interaction in a Tb glass target comprised of 15 μm fibers of 1.0 cm length. The neutron event was recorded in the P-East beam (E400) at Fermilab, the pion event at the SLAC test beam. From such data frames and others we conclude that tracks and interactions are indeed clear and distinct for both nuclear fragments (dark tracks) and minimum ionizing particles (light tracks) in fiber-optic plates containing scintillating glass fibers of very small cross section (10-25 μm) and fiber depths of ~1 cm. Spatial resolution is good $\sigma \lesssim 30$ μm per measured point, and we observe ~5 detected photoelectrons per mm of path length for minimum ionizing particles in Tb glass and ≳2 for Ce glass.

We are currently studying light attenuation in fibers longer than a few centimeters, the radiation resistance of the glass[2], and are exploring new glass compositions in order to improve the tracking response[3]. The immediate goal is to provide a working tracking detector for Fermilab E687 (photoproduction of high mass states at the Tevatron) and to develop large scale devices for colliding beam experiments.

We would like to thank the staffs of SLAC and Fermilab and the experimenters of Fermilab E400 for help with the beam tests.

*This work has been supported in part by grants from the U.S. National Science Foundation and the University of Notre Dame.

REFERENCES

1. R. Ruchti et al., IEEE Transactions on Nuclear Science, Vol. NS-31, No. 1 (1984), pp. 69-73.
2. Cerium glass is extremely radiation resistant. See B.D. Evens and G.H. Sigel, IEEE Transactions on Nuclear Science, Vol. NS-22, No. 6 (1975), pp. 2462-2467.
3. Present estimates indicate an improvement of a factor of ~4 in performance of Cerium targets incorporating a refined imaging system.

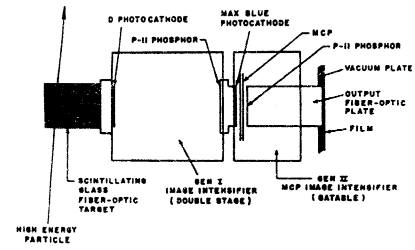

Fig. 1. Schematic of Target and Imaging System

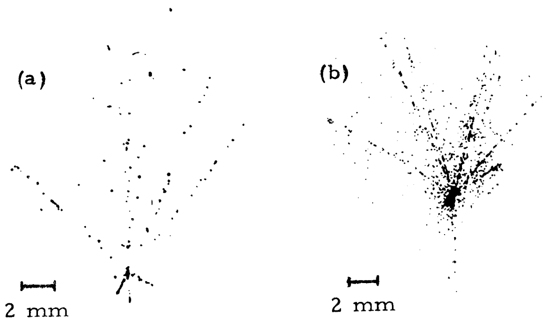

Fig. 2. Interactions recorded in scintillating glass fiber-optic targets: (a) ~600 GeV/c neutron in Ce glass; (b) 10 GeV/c π^- in Tb glass.

CONSTRUCTION AND TEST OF A PROTOTYPE ELECTROMAGNETIC CALORIMETER USING PLASTIC SCINTILLATING FIBERS IMMERSED IN A BISMUTH LEAD ALLOY

Henry BLUMENFELD
CEN - SACLAY
DPhPE - STIPE
91191 GIF sur YVETTE Cedex, France

I. INTRODUCTION

A group at Saclay has conceived of a new approach to the design of an electromagnetic shower calorimeter using plastic scintillating fibers immersed in a low melting point high density alloy with the fibers pointing along the general direction of the showering particles.

II. CONSTRUCTION

Approximately 4 km of clad scintillating fibers 1 mm diameter (0.8-1.1 mm) were drawn in Saclay. The characteristics of the fibers are as follows : a polystyrene core with a refractive index n = 1.59, a cladding about 10 μ thick with n = 1.46, a light emission centered at λ = 430 nm and an attenuation length going from 30 to 300 cm depending on the distance from the excitation. The fibers were disposed continuously in sheets of 80 fibers covering a metal screen 0.5 mm thick and 80 such sheets were piled on top of each other to give an useful cross section inside the mold of 80 x 120 mm and a length (inside the wold) of 265 mm. An alloy melting at 71°C (AFBAT : Bi 49.5%, Pb 27.5%, Sn 13.2%, Cd 10%) was then poured at 80°C to fill completely the alloted volume.

The overall density of the block came out to be D = 5.3 g/cm^3 with a radiation length X_o = 14.5 mm and a filling factor for the fibers of 0.51.

At first we left 20 cm of fibers protruding at one end, tied in a bundle of 110 mm diameter, impregnated with epoxy resin on the extreme 2 cm and polished for good optical contact with a photomultiplier tube (P.M.). For later tests we cut the protruding fibers flush and placed the P.M. tube directly on the polished exit face. The other side (beam entrance) was polished and we applied a reflecting "Scotch" tape to it.

III. TEST RESULTS WITH BEAM

The block was tested at CERN with electron beams from 5 to 25 GeV. For most tests described here a parallel test was performed with a CEREN 32 lead glass block.

III.1 - Spatial Scan

We scanned the fiber block in an electron beam about 1 cm in diameter, performing a horizontal and vertical scan at 0° and 10° to check the uniformity of response. The block was always positioned with the wide dimension as the base and the rotation being around a vertical axis. We observed a plateau of about 5 cm, uniform to ± 10%. We also performed a scan of the block turned at 90° with respect to a 25 GeV pion beam. The response to this test indicates that the structure of the block is homogeneous and that the attenuation length of the fibers in the block does not differ appreciably from that of the bare fibers.

III.2 - Energy Scan

We performed an energy scan with a 5 inch P.M. (RTC XP 2050). The response is linear with energy within the measurement errors and the straight line fit passes close to zero. From the calibration we determine that we collect approximately 4600 photoelectrons per GeV, (with the P.M. placed directly against the exit face). The reflective tape contributes about 25% to this number. The signal was 2.1 times larger than with the lead glass block used with the same P.M.

We also determined, by using a π^- beam, that 11 ± 2% of the shower energy is dissipated in the fibers. This has an important bearing on the resistance to radiation dammage.

We tested that one has a sufficient amount of light to use a photodiode or phototriode tube allowing an operation in a magnetic field of the order of 1 Tesla.

III.3 - Energy Resolution

The energy resolution $\sigma/\sqrt{E}$ varies from 9 to 13% in GeV$^{1/2}$ (r.m.s.) for an energy going from 5 to 25 GeV and an incident angle between 5 and 25 degrees. Only at zero degree is the energy resolution appreciably deteriorated.

III.4 - Reduction in Surface

The fibers fill one half the volume of the block. It becomes therefore possible to group the fibers emerging from the block thus reducing by a corresponding factor the active light sensitive reading area (P.M. or phototriode).

Another important gain in area can be obtained using the fact that the light in the fibers is transmitted in a cone of half opening angle of 24 degrees. Using a plastic "semi-adiabatic" light guide we obtained reduction in light of 23% for an area reduction of a factor of 3.

III.5 - Shower Localization

We carried out a preliminary attempt to measure the transverse position of the shower. The error we found on this position is of the order of ± 2 mm with a 20 GeV electron beam.

IV. RADIATION RESISTANCE

We have observed that it takes a dose of 3 x 10^6 rad. to reduce the attenuation length of the bare fibers by a factor of two. Since only about 10% of the shower energy is deposited in the fibers one can extrapolate that it should be possible to subject the alloy-fiber block to doses of 3 x 10^7 rad.

V. FUTURE DEVELOPMENTS

V-1. We are testing methods for a more efficient production of the fiber blocks. In particular we have successfully tested industrial weaving techniques which greatly facilitate the ranging of the fibers.

V-2. A company by the name of OPTECTRON (zone industrielle de Courtaboeuf, 91 - ORSAY, France) has been established near Saclay to carry out the industrial production of plastic optical fibers.

A FACILITY FOR INVESTIGATION OF MULTIPARTICLE PRODUCTION AT COSMIC-RAY ENERGIES

Torsti, J.J. , Valtonen, E., Arvela, H., Lumme, M., Nieminen, M., Peltonen, J., and Vainikka, E.

University of Turku
Wihuri Physical Laboratory
20500 Turku, Finland

and

University of Turku
Department of Physical Sciences
20500 Turku, Finland

A cosmic-ray hadron spectrometer capable of measuring the energy spectrum of hadrons at sea level in the range 0.01 - 1000 GeV has been operated for several years at the University of Turku in Finland /1/. During the measurements it appeared that simultaneous incidence of multiple hadrons severely distorts the results above about 100 GeV. Simulations of atmospheric hadron cascades showed that the occurrence of multiple hadron events increases with detected energy and is strongly dependent on the detector area /2/.

An improved experimental arrangement for studying multiple production of hadrons in high-energy hadron-air-nucleus collisions is now under construction. The front view of the improved spectrometer is shown in figure 1. The main parts of the instrument are plastic and liquid scintillators and a double neutron monitor for measurement of energies of incident hadrons and streamer tubes as position-sensitive detectors. The total depth of the spectrometer is about 6 inelastic mean free paths of high-energy hadrons (λ). The depth of lead is about 3λ, and that of iron and light materials (mostly paraffin) 1.25λ, and 1.75λ, respectively. Energies of incident hadrons are determined by combining two methods. The energy of the electromagnetic shower produced by an incident hadron in the absorber layers is measured calorimetrically by means of the liquid scintillators. On the other hand, the multiplicity of low-energy neutrons produced by the hadron in nuclear collisions in the two lead targets is measured by the neutron monitors. Each monitor records the multiplicity independently. The energy resolution of the spectrometer will be about 30 - 40 %. The threshold energy for detecting charged particles is below 1 GeV and the maximum detectable energy is about 2000 GeV.

Three layers of streamer tubes will be used for determining the number of simultaneously incident charged particles (fig. 1). The streamer tubes are of the same type as those described by Iarocci /3/. Active area of each layer is 5.5 m^2. The anode wires of tubes in successive layers make an angle of 30 degrees with respect to each other. Two-dimensional digital readout from each tube plane by perpendicular induction strips enables the position of incident particles to be determined with an accuracy of 10 mm and the arrival direction of particles with an accuracy of 2 degrees.

A small air shower array will be constructed in connection with the spectrometer. The quantities to be measured are the core position, size, and arrival direction of a shower. The core position is determined by four core detectors applying the method proposed by Bergamasco et al. /4/. The measurement is based on relative pulse heights of two scintillators one on top of the other and separated by a lead layer. Three additional scintillators on the corners of an equilateral triangle with sides of about 17 m will be equiped with fast photomultipliers to do the timing necessary for the determination of the arrival direction of the shower.

By using the experimental arrangement described above, energy spectra of groups with various numbers of charged particles can be measured. In addition, the lateral distribution of particles belonging to the same group can be determined. Particles detected over an area of 1 m^2 at sea level are produced in high-energy hadron - air-nucleus interactions at the height of about 600 - 800 m in the atmosphere. These particles are emitted in angles less than 2 mrad with respect to the primary particle direction. The results obtained in this experiment thus give information on multiparticle production and correlations therein at very low transverse momenta. The primary energy range covered by the experiment is from 1 TeV to about 1000 TeV.

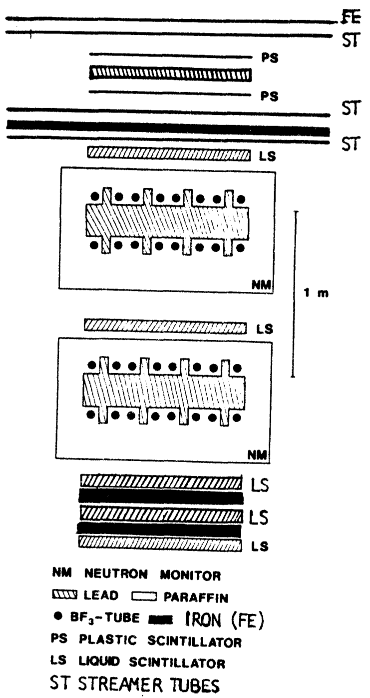

Fig. 1. Front view of the improved spectrometer.

Experimental studies of the occurrence of multiple hadron events are of considerable significance in order to understand some features of hadron component in air showers, e.g., the number of hadrons per shower, the energy spectrum, lateral distribution, and charged to neutral ratio of hadrons. In addition, multiparticle correlation effects are sensitive to the model of particle production and thus give additional information on high-enrgy hadron - nucleus interactions.

/1/ Nieminen, M. et al. Phys. Rev. D 26, 1036 (1982).
/2/ Arvela, H. et al. J. Phys. G 10, 695 (1984).
/3/ Iarocci, E. Nucl. Instrum & Methods 217, 30 (1983).
/4/ Bergamasco, L. et al. Nuovo Cimento 2C, Ser 1, 453 (1979).

EXPERIMENTAL SET-UP USED TO STUDY INTERACTIONS OF RELATIVISTIC NUCLEAR FRAGMENTS AT THE DUBNA SYNCHROPHASOTRON

V.Dodokhov, S.Dolya, A.Fedunov, I.Golutvin, N.Gorbunov, A.Karev, V.Karzhavin, V.Khabarov, V.Lysyakov, B.Morozov, V.Nakhratsky, V.Nikitin, V.Perelygin, Yu.Petukhov, A.Popov, A.Povtoreiko, D.Pose, V.Sarantsev, D.Smolin, L.Svetov, A.Sukhanov, V.Sviridov, V.Tikhomirov, V.Tokarsky, I.Veress, Yu.Yatsunenko, A.Zarubin, V.Zhiltsov
Joint Institute for Nuclear Research
Department of New Methods of Acceleration, Dubna, USSR

A method[1] and a detector that permit one to analyse the anomalon's phenomenon in nuclear interactions[2] with a high statistical accuracy are described. An experimental set-up was exposed to ^{12}C, ^{16}O, ^{22}Ne and ^{24}Mg beams at the Dubna synchrophasotron at an energy of up to 4.5 GeV/c.A. A layout of the experimental set-up is shown in Fig.1, where PC1-8 are proportional chambers; S1-5 scintillation counters and C1-40 Cerenkov counters. A principal part of the apparatus is the target-detector.

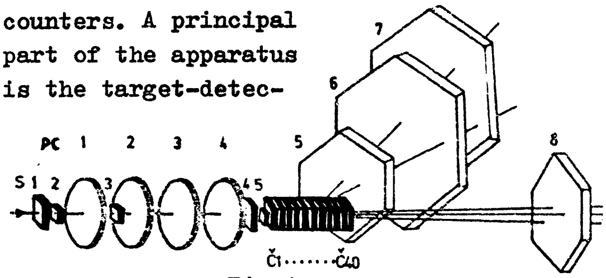

Fig.1.

The detector represents a stack of 40 Cerenkov counters. Each plexiglass radiator 0.52 cm thick is connected to a PM ФЭУ-84. The pulse height of a Cerenkov signal is proportional to the ion charge squared. There is a total internal reflection of Cerenkov light in the radiators if the angular deflection of an ion with a momentum of 4.2 GeV/c.A relative to the beam axis is no more than 2.5°[3]. The Cerenkov stack permits one to determine the coordinates the point of fragment production and their interaction by measuring a charge change in the counters in series. The display of a typical event in Cerenkov stack is shown in Fig.2. Proportional chambers PC1-4 are used to measure the coordinates of the tracks of projectile ions. Each module contains 3 planes of sense wires rotated to 60° with respect to each other.

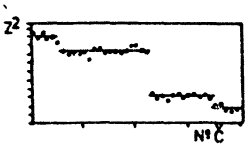

Fig.2.

The sensitive regions of the chambers are: PC1-4 - 128 mm, PC5,8 - 384 mm, PC6 - 640 mm and PC7 - 896 mm. The signal wire spacing is 2mm. An aluminium foil 14µm thick is used for HV cathodes. Fig.3 shows the efficiency of the beam chambers PC1-4 for relativistic ions with charges from Z=1 to 12 vs high voltage setting. The accuracy in measuring the entry point of projectile ions is 0.4 mm.

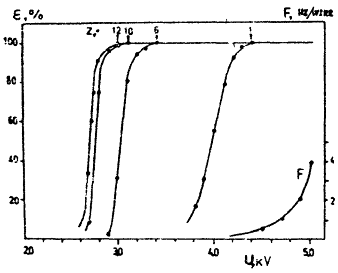

Fig.3.

The telescope of 5 scintillation counters, placed in front of target, provides a trigger. The average resolution of a Cerenkov counter is 0.25 e for Z=10. This resolution ensure sufficient fragment separation. Fig.4 shows the Z^2

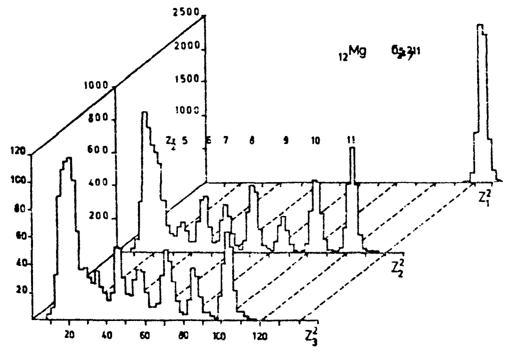

Fig.4.

distribution for ^{24}Mg - (Z_1^2) and its fragments with a > 3.5 cm free path for the second - (Z_2^2) and third generations - (Z_3^2). A remarkable feature of the Cerenkov spectrometer is its almost complete insensitivity to slow and strong ionizing secondary particles and low sensitivity to relativistic particles deflected considerably (more than 2.5°) from the beam axis. The set-up permits one to separate fragments sufficiently, to suppress accompaning particles, to measure the fragmentation branching and the mean free path of nuclei and their fragments. For a single interaction the accuracy in determining the vertex is about 3 mm. The accuracy in measuring the mean free path of nuclei is 2.0% for ^{24}Mg.

1. Golutvin I.A. et al., P1-83-85, Dubna, 1983.
2. Friedlander E.M. et al. PRL, 45, 1084, 1980.
3. Volkov V.I. et al. B1-83-854, Dubna, 1983.

INSTRUMENTATION AT LARGE HADRON COLLIDERS

E Radermacher

III. Physikalisches Institut A

Technische Hochschule Aachen
Fed. Rep. Germany

1) <u>Introduction</u>: When C. Rubbia et al. [1] proposed in 1976 the conversion of the existing CERN SPS accelerator into a proton-antiproton collider with $\sqrt{s}$ = 540 GeV, the main purpose was the observation of the intermediate vector bosons $W^{\pm}$ and Z^{o} with masses > 80 GeV/c^2 predicted by the unified gauge theories [2]. In addition other physics, like quark and gluon interactions, Drell-Yan processes, production of heavy flavours and Higgs bosons, and new phenomena could be studied in an yet unknown energy range. The Sp$\bar{p}$S collider is running since 1981 and has so far collected data for 136 nb^{-1} integrated luminosity.

A new $\bar{p}$p project started at Fermilab. It foresees $\bar{p}$p collisions for 1986 with $\sqrt{s}$ = 2 TeV.
In order to achieve the important physics goals the main aspects of a detector become clear:

i) It should be as hermetically closed as possible, thus detecting all reaction products.
ii) It should be capable of detecting the charged leptons: the electrons by their electromagnetic shower cascade and the muons by their penetrating capability through a large amount of material.
iii) It should visualize all charged tracks and measure their momenta by a magnetic analysis.
iv) It should measure the energy of the particles by calorimetry. This should provide a detection of the neutrino, identified by the missing energy.
v) A separation of electromagnetic particles from hadrons should be possible.

All this leads to a general-purpose detector capable of coping with all kinds of physics.

2) <u>The detectors at the CERN Sp$\bar{p}$S</u>: Six experiments [3] have been approved for the $\bar{p}$p collider at CERN. Before describing in detail the UA1 and UA2 experiments, let us briefly mention the other experiments. The UA3 experiment searches for magnetic monopoles by measuring the ionization loss in 125 μm Kapton foils fixed on the vacuum tube and the UA1 central detector. The UA4 experiment measures the $\bar{p}$p elastic scattering and total cross section by using so-called "Roman pots" located 40 m away from the interaction point. Two large streamer chambers are used by the UA5 experiment to measure the general features of $\bar{p}$p collisions. The UA6 experiment is not directly a collider experiment since it observes collisions of the p and $\bar{p}$ beams at $\sqrt{s}$ = 22.5 GeV with a hydrogen jet target.

2.1 <u>The UA1 detector (see fig. 1)</u>: It covers almost completely the whole solid angle down to Θ=0.2^o [4].

The centre piece ($5^o<\Theta<175^o$) is a drift chamber, a cylindrical volume 5.8 m in length and 2.3 m in diameter. This central detector (CD) has 6110 sense wires and is located in a dipole magnet generating a field of 0.7 T which is horizontal and perpendicular to the beam. The CD is a self-supporting cylinder made of six independent half-cylinder chambers. The drift distance of 18 cm has been chosen, so that the total drift-time of 3.6 μs is less than the time between two $\bar{p}$p collisions (3.8 μs). The CD has two types of read-out: drift-time measurement and charge-division method. In addition the energy loss dE/dx is measured. The overall spatial resolution is of the order of 290 μm in the drift-time coordinate and 1.7% of the wire length for the charge-division coordinate. This results in a momentum accuracy of $\Delta p/p = 5\times10^{-3}p$.

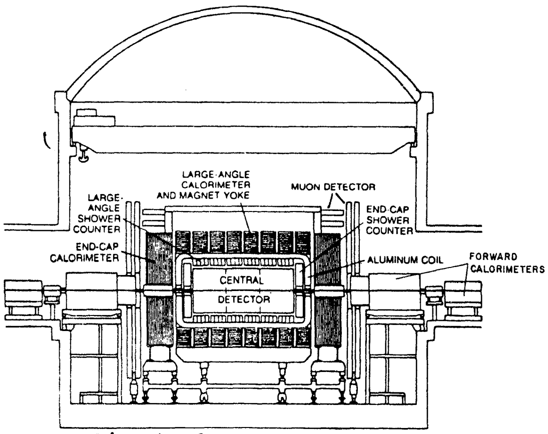

Fig. 1: The UA1 detector

Various calibrations are done to provide a knowledge of the drift velocity, drift angle, reference time t_o and wire position by using an electronic test-pulse system, X-rays and ionizing laser beams.
Next to the CD is the electromagnetic calorimeter, still inside the magnet. It consists of two parts:
i) a cylindrical calorimeter, 6 m long with an inner diameter of 2.72 m, covers the region $25^o<\Theta<155^o$. It consists of 48 semicylindrical half shells, 24 on each side of the beam ($\Delta\Theta = 5^o$, $\Delta\phi = 180^o$). Alternating layers of scintillator (1.5 mm) and lead (1.2 mm) form four segments in depth with the following radiation lengths: 3.3/6.6/9.9/6.6 X_o. By pairing the right photomultipliers of each half shell one obtains an azimuthal resolution of $\sigma(\phi) = 0.24/\sqrt{E}$ rad and a resolution of the coordinate along the beam of $\sigma(x) = 6.3/\sqrt{E}$ cm (E in GeV). Using an electron test beam for calibration one determined the energy resolution to $\sigma(E) = 0.15\sqrt{E}$ GeV. In addition it was found out that 98% of all electrons deposit less than 1% of their energy in the subsequent hadron calorimeter. The energy calibration is performed periodically with a 7 Ci ^{60}Co source and the stability of the photomultiplier gain is monitored by a laser system.
ii) The end faces of the CD are covered by end-cap calorimeters ($5^o<\Theta<25^o$ and $155^o<\Theta<175^o$). Each one is divided into 16 equal sectors ($\Delta\Theta=20^o$, $\Delta\phi=11^o$). Each sector, a sandwich of lead (4 mm) and scintillator (6 mm) is segmented into four parts in depth: 3.6/7.2/8.7/7.2 X_o. The attenuation length of the scintillator has been chosen so as to measure directly $E_T = E\sin\Theta$. After the first two segments a position detector is located to measure the shower position.

The hadron calorimeter ($5^o<\Theta<175^o$) is formed of two types of modules: in the central region one finds 16C-shaped modules as return yoke of the magnet, in the front region 12 I-shaped modules. The calorimeter is of the iron/scintillator sandwich type: 1 cm scintillator and 5 cm iron plates repeated 16 times. The modules are subdivided in two equal parts in depth and in polar and azimuthal angle: $(\Delta\Theta,\Delta\phi) = (15^o,18^o)$ for the C-modules and $(\Delta\Theta,\Delta\phi) = (5^o,10^o)$ for the I-modules. Using test beams of hadrons, the resolution was found to be $\sigma(E) = 0.8\sqrt{E}$ GeV.
In order to complement the electron identification over as large a solid angle as possible, fifty muon

chambers, nearly 4m x 6m, surround the whole detector. Each chamber consists of two orthogonal layers of drift tubes with two planes per projection. With a staggered arrangement for adjacent planes one resolves the left-right ambiguity. The extruded aluminum drift tubes have a cross-section of 45 mm x 150 mm, leading to a maximum drift length of 70 mm. Tests in a beam and with cosmic-ray muons have shown that an average spatial resolution of σ = 300 μm is achieved. The muon detector itself provides a trigger on high-momentum muons requiring a track pointing to the interaction vertex within ± 150 mrad (decision time: 1μs after maximum drift-time).
Additional calorimetry, both electromagnetic and hadronic, and track detection extend to the forward regions of the experiment, down to 0.2°.

2.2 The UA2 detector (see fig. 2): This detector [4] is instrumented to identify electrons and measure their energy over a polar angle interval $20^o<\Theta<160^o$. This central region has no magnetic field. Only for $20^o<\Theta<37.5^o$ and $142.5^o<\Theta<160^o$ are there magnetic spectrometers.

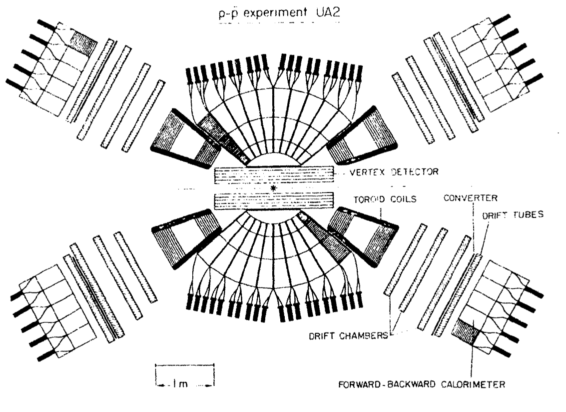

Fig. 2: The UA2 detector

The vertex detector, surrounding the p̄p interaction point, is a system of cylindrical chambers:
i) Four multiwire proportional chambers, with digital read-out on 2112 anode wires and analog read-out on 2160 cathode strips, at ±45° with respect to the wires.
ii) Two large-gap drift chambers, with 12 sense-wire planes measuring the track position by charge division to 1% of the wire length. These chambers determine the position of the event vertex along the beam line with a precision of ± 1 mm and the ionization loss to 20%. The vertex detector is surrounded by a 1.5 radiation lengths tungsten converter followed by a proportional chamber, the pre-shower counter. It localizes the electromagnetic showers initiated in the tungsten with a precision of 3 mm.
The central calorimeter contains an electromagnetic and a hadronic part and covers the full azimuth and a polar angle interval $40^o<\Theta<140^o$. It is segmented into 240 cells ($\Delta\Theta = 10^o$, $\Delta\phi = 15^o$). Each cell is segmented in three longitudinal sections:
1) the electromagnetic compartment, 17.5 X_o deep, consists of 26 lead plates (3.5 mm) and 27 scintillator plates (4 mm).
ii) two hadronic compartments, each roughly 2 absorption lengths deep, is made of 15 mm thick iron plates interspaced by 5 mm thick plates of acrylic scintillator.
Each cell has been calibrated in a testbeam using electrons for the electromagnetic calorimeter and muons for the hadronic one. The calibration stability has been measured continuously by a light-flash system, using a Xenon flash tube, and a movable 4mCi ^{60}Co source, running along the front faces of the calorimeter. The systematic uncertainty in the absolute energy scale is less than ± 1.5% for the electromagnetic and less than 3% for the hadronic calorimeters. The e.m. energy resolution was measured to be $\sigma(E) = 0.14\sqrt{E}$ and it turned out that, at 70 GeV energy, 95% of all electrons deposit less than 11% of their energy in the first hadron calorimeter. The resolution in the hadron calorimeter decreases from ∿ 30% at 1 GeV to ∿ 13% at 70 GeV, approximately proportional to $E^{-1/4}$.
The two forward regions are each equipped with twelve toroidal magnet sectors having a mean-field integral of 0.38 T.m. Each sector is instrumented with:
i) three drift chambers with three sense wires planes each (-7°, 0°, +7°) having a point resolution on tracks of σ_p = 200 μm and an angular resolution in the bending plane of σ_t = 0.47 mrad.
ii) a 1.4 X_o lead-iron converter, followed by a multitube proportional chamber of trapezoidal shape with three layers (-7°, 0°, +7°) of drift tubes and two planes per projection.
iii) an electromagnetic calorimeter of the lead-scintillator sandwich type, subdivided into 10 independent cells. The energy resolution is $\sigma = 0.15\sqrt{E}$ GeV and the calibration stability is better than 3%.

2.3 The performance of the detectors: Their main task is the observation of high p_T leptons originating from the decays of the $W^\pm$ and Z^o bosons.
Isolated electrons are identified by their characteristic transition curve, and in particular by the lack of penetration in the hadron calorimeter. In addition a track from the central detector must point to the electromagnetic cluster and in the case of a magnetic field the measured momentum must coincide with the measured energy.
Neutrinos identify themselves by the apparent visible energy imbalance (missing energy). Here the calorimetry down to 0.2° in polar angle Θ is important in the case of the UA1 experiment.
The muons are identified in the UA1 detector after penetration of the 6.1/sinΘ absorption lengths of the calorimeters and the additional iron shielding (40 cm on the top, 60 cm on the side) in front of the muon detector. To be accepted as a muon candidate, the extrapolated CD track must agree in position and angle with the one measured in the muon chamber.

Both detectors unambiguously identified in 1983 the $W\to e\nu$ and $Z^o\to e^+e^-$ decays, and the UA1 detector in addition the muonic channels [5]. The average mass values [4] are $m_W = 82.1\pm1.7$ GeV/c^2 and $m_{Z^o} = 93.0 \pm 1.7$ GeV/c^2 in excellent agreement with the prediction of the SU(2) x U(1) model.

3) The upgrading of the detectors: The search for the top quark is the most interesting challenge, even if there might be already today some positive indication for it [6]. Also the search for the Higgs particle is most important. Better determination of the $W^\pm$ and Z^o parameters by improved calorimetry test further the standard model. Observation of heavy leptons, SUSY particles, additional $W^\pm$ and Z^o etc. is another purpose of the detectors.
An upgrading program has been proposed by the UA1 group [7] which consists in the following modifications:
i) magnetization of the side and top iron shielding and instrumentation with streamer tubes. This independent momentum measurement helps to identify μ's by comparing their momenta in the CD and outside, and reduces therefore the $K\to\mu\nu$ decay contribution. The streamer tubes are made out of PVC coated with conductive (graphite) vanish, the readout is done by 12 mm wide strips orthogonal to the tubes. First tests with a Fe^{55} source gave a resolution of $\sigma(x) \leq 250$ μm over the strip width.
ii) Implementation of additional iron ($\leq$ 120 cm) in the forward region. This might reduce the muon trigger rate by a factor 10 and increases considerably the acceptance for $W\to\mu\nu$ and $Z^o\to\mu^+\mu^-$ decays. The adding of streamer tubes is also planned.
iii) Installation of a microvertex detector together with a Be beam pipe. Owing to the relatively large bottom-quark lifetime of $\tau \sim 10^{-12}$ s, the secondary vertex in the $W \to t\,\bar{b}$ decay is ∿ 1.8 mm away from the primary vertex. Also the secondary vertices for the

decay of the Higgs-particle into $c\bar{c}$ or $b\bar{b}$ might be visualized using a pressurized high precision drift chamber. Using the Isajet Monte-Carlo and considering the multiple scattering in the Be beam pipe, the single wire accuracy and the number of sense wires, it turned out, that for 25 µm single wire accuracy, the probability to detect $\geq$ 1 vertex with 90% C.L. is 45 - 60%. The proposed microvertex detector is of jet like structure with staggered sense wires of 23 µm NiCoTi parallel to the beam. The inner radius is 26.5 mm, the outer radius 85.8 mm and the length is 85 cm. The cathode wires (100 µm CuBeAu) are varied from 12.6 kV (outer radius) to 5.7 kV (inner radius) so that the equipotential lines (E/p = 1.5 kV/cm.atm) are parallel to the sense wire planes. First tests at 4 atm with Ar(90%) + CO_2(9%) + CH_4(1%) gave a resolution of $\sigma = 40\mu$ for 3 consecutive wires using the drift time and $\sigma \approx 2$ cm for the current division.

iiii) Whilst all the above improvements will be made in 1984 or early in 1985, the UA1 collaboration will replace the electromagnetic calorimeter in a long term program by an U calorimeter, used for electromagnetic and hadronic energy measurements. In fact, the difference in response for e.m. and hadronic showers of ordinary calorimeters (e/p = 1.4) represents the main uncertainty in the jet energy and missing energy determination. By using depleted Uranium one makes use of the fission amplification [8], resulting in a compensation, i.e. e/p → 1 and improving considerably the resolution. In fact using liquid Argon as electron collector leads to $\sigma = 0.3 \sqrt{E}$ GeV for hadronic showers and $\sigma = 0.1 \sqrt{E}$ GeV for electromagnetic showers. But using liquid Argon in the UA1 detector would considerably spoil the good hermeticity due to cryogenics. Therefore it is planned to use tetramethylsilane (TMS) at room temperature. It has the nice feature that not only the fission γ rays are used for compensation as in liquid argon but also neutrons from fission and spallation. The main contribution of the energy deposition is coming from spallation neutron induced proton recoils due to the hydrogen atoms in the TMS [9]. One problem with TMS is the oxygen impurity which stops the electron drift. But one succeeded to purify TMS even in large quantities, so that the drift could be observed [10]. The first U plates arrived at CERN and a test-module is under construction.

Also the UA2 group proposed an upgrading [11] of their detector consisting in the following changements:

i) Replacement of the forward detectors by end cap calorimeters down to $\Theta = 5^{\circ}$ in order to achieve a better missing energy measurement. It will be of the same type as the central calorimeter. This means giving up the measurement of the charge of the particles, e.g. the electrons from the W decay.

ii) one aims getting a better rejection against background for small transverse momentum electrons, e.g. from the semileptonic decay of the b or t quarks. Converted photons from π^0-decays and unresolved π^0-π^+-pairs constitute the main background. Therefore one installs a Be beam pipe and the first two proportional chambers in the central region will be replaced by four other proportional chambers with annular cathode strips and a silicon counter, consisting of 432 Si detectors. Each detector has an area of 0.9 cm^2 and overlaps with its neighbours in order to reduce the insensitive area. First tests with a ^{106}Ru source showed a satisfactory performance.

4) The detectors at Fermilab: When the $\bar{p}p$-project at Fermilab will start in 1986 with $\sqrt{s}$ = 2 TeV, two detectors are foreseen to collect data. The cross sections are an order of magnitude higher than at the CERN $S\bar{p}pS$ collider and masses of 200 - 500 GeV/c^2 can be produced. The proposed detectors are quite similar to those at CERN.

4.1 The CDF detector [12]: In the central part ($10^{\circ} < \Theta < 170^{\circ}$) there will be a 1.5 T superconducting solenoid. A central tracking chamber will record the image of the events. It is followed by an electromagnetic calorimeter divided in 480 cells ($\Delta\phi = 15^{\circ}$, $\Delta\Theta = 6^{\circ}$) of the lead scintillator sandwich type with a total thickness of 20 X_0. The first tests gave an energy resolution of $\sigma(E) = 0.14 \sqrt{E}$ GeV. Next comes an iron/scintillator hadron calorimeter of 5 absorption lengths. The whole central part is covered by muon chambers. The end faces of the central region are equipped successively by an intermediate tracking chamber, an end plug shower counter and an end plug hadron calorimeter. In the forward region ($2<\Theta<10^{\circ}$) there is a e.m. and hadronic calorimeter with tracking chambers. In the backward region ($170^{\circ} < \Theta < 178^{\circ}$) there is the same detector and in addition iron toroids and drift chambers for muon detection.

4.2 The Dϕ detector [13]: There is no magnetic field in the central region, thus allowing a more compact detector which can cover the full solid angle. The central tracking system consists of three separate subsystems in angular coverage, a central cylindrical drift chamber and two end track sections. All three chambers have an outer and inner region and between them are located transition radiation detectors. The radiator is made out of polyethylen fiber followed by multiwire proportional chambers (Ar: 50%, Xe = 50%) as X-ray detector. The calorimetry, after the tracking system is done by an U/liquid Ar calorimeter divided in the e.m. part into four segments (2/2/6/14 X_0) and in the hadronic part also in four segments (1/1.4/1.8/2.0λ). The expected energy resolutions are respectively $\sigma = 0.11 \sqrt{E}$ GeV and $\sigma = 0.37 \sqrt{E}$. The muon identification and momentum measurement is accomplished with iron toroids, excited to a mean field of 20 KG followed by planes of proportional drift tubes.

5) Conclusion: The experiments of the CERN $S\bar{p}pS$ collider have greatly fulfilled their duties. Unexpected events, yet unobserved particles, the better knowledge of the detectors and the new accumulator ACOL make an upgrading necessary in the next years. The Tevatron detectors took profit from the learning procedure with the $S\bar{p}pS$ detectors and designed their detectors accordingly. It remains now to wait for the new physics to appear.

References

1) C. Rubbia, P. McIntyre and D. Cline, Proc. Int. Neutrino Conf., Aachen, 1976 (eds. H. Faissner, H. Reithler and P. Zerwas) (Vieweg, Braunschweig, 1977), p. 683
2) S.L. Glashow, Nucl. Phys. 22 (1961) 579
S. Weinberg, Phys. Rev. Letters 19 (1967) 1264
A. Salam, Proc. 8th Nobel Symposium, Aspenäsgarden, 1968 (ed. N. Svartholm) (Almqvist and Wiksell, Stockholm, 1968) p. 367
3) UA1 proposal, CERN SPSC 78-6/P 92 (1978)
UA2 proposal, CERN SPSC 78-8/P 93 (1978)
UA3 proposal, CERN SPSC 78-15/P 96 (1978)
UA4 proposal, CERN SPSC 78-105/P 114 (1978)
UA5 proposal, CERN SPSC 78-10/P 108 (1978)
UA6 proposal, CERN SPSC 80-63/P 148 (1980)
4) For a general description of the UA1 and UA2 detectors and the experimental discovery of the W and Z bosons, see E. Radermacher, CERN-EP/84-41, and all references quoted therein.
5) G. Arnison et al., Phys. Letters 122B (1983) 103
M. Banner et al., Phys. Letters 122B (1983) 476
G. Arnison et al., Phys. Letters 126B (1983) 398
P. Bagnaia et al., Phys. Letters 129B (1983) 130
G. Arnison et al., Phys. Letters 134B (1984) 469
6) R. Böck, contribution to this conference.
7) The UA1 Collaboration, CERN/SPSC/82-51, P92, Add. 2; 83-48, P92, Add. 3; 83-79, P92, Add. 4
8) C.W. Fabian et al., Nucl. Inst. and Methods 141 (1977) 61
9) A. Di Ciaccio, M. Goodman, private communication
10) J. Engler, H. Keim, Report KfK 3638, Dec. 1983
R.C. Muñoz, Thesis Purdue University, August 1983
D. Schinzel, private communication
11) UA2 Collaboration, CERN/SPSC/84-30, P93, Add. 2
12) CDF Collaboration, Design report August 1981
13) Dϕ Collaboration, Design report, December 1983

POSSIBILITIES AND LIMITATIONS OF GASEOUS DETECTORS

H. G. FISCHER
CERN
GENEVA, SWITZERLAND

Let me start by using the nice title of my talk (which would, by the way, merit a several-hours seminar) for some disrespectful meditations on status and future of gaseous detectors in high-energy physics.

As far as the possibilities are concerned, they are of course given by the physics of gaseous electronics and by the energy loss of relativistic particles in matter. As such they are known since many years, if not generations. Indeed very few new detector ideas are younger than a decade or two.

On the other hand most of us seem to be engaged in a desperate race to find the limitations of gaseous detection, both on the quantitative level of mere detector size and on the qualitative one of basic detector physics. Again one might claim that at least the second class of limitations should be known since a very long time.

However, gaseous electronics is a field of physics that has seen its heyday a considerable time ago and very little has been added in basic research over the rather hectic years of exploitation for high-energy physics. In addition, the limitations - like most unpleasant facts of life - have the somewhat unfortunate tendency to be forgotten (and painfully rediscovered) in periodic intervals.

The fact that relatively little time and money are actually spent for detector research is often a source of frustration for the detector builder. It is also certainly a source of losses in funds, effort and physics possibilities in a field that has seen an incredible increase of detector size and expenditure over the past few years.

In this environment it is not surprising to find a relatively small number of dedicated individuals at the origin of most new detector developments. In this sense modern gaseous detection set off with the rediscovery, by G.Charpak, of the proportional regime of gas amplification and his development of the multiwire proportional chamber. Immediately after this first step, there was a real proliferation of ideas such that even the most sophisticated applications in use today have their roots in the early 1970's.

It is, however, a long way from a new detector idea to its realization in a large-scale experiment: this is where the limitations come in very severely. It took some time to understand that the development of new, especially of "limiting" detectors is a long-term adventure that may well take a decade or so. The problem is of course compounded by the simultaneous rapid increase in detector size and complexity and by the fact that the lead time given by accelerator availability or the mean life of an experiment seems to stay fixed at a few year's level. As a consequence, a rather conservative attitude of the "broad public" towards detector novelties ensues.

The time scale involved can be studied in a number of developments like large-volume imaging chambers (TPC), large-scale energy-loss sampling devices (ISIS), ultrafast time-measuring devices (Pestov-counters), detection of Cerenkov radiation (RICH) and so on. Most of these have been proposed in the early 1970's and come to fruitation now.

Let me summarize this introduction in four points:

- The time scale for "limiting" detector techniques is long.
- The progress in gaseous electronics is slow.
- High energy physics experiments unify and concentrate into a small number of rather standard but very large and complex detectors.
- The time scale given for the realization of these detectors seems to be invariant and independent on size or complexity.

I will now try to give an idea on the status of gaseous detection with some emphasis on limitations. Since it will be impossible to do justice to the whole field in the few minutes of my talk, I would like to invite you to two little races. The first race will take us through the microscopic realm of the basic detection process. The second one will address the macroscopic world of some "limiting" detectors.

FIRST RACE: Basic Detection Process

We will follow the detection process from its initialisation by ionization up to the collection of the positive ions at the cathode.

Ionization

The description of the energy-loss distribution resulting from ionization (which is in gases generally not a Landau distribution) has found a rather satisfactory solution by Monte Carlo methods. The available approaches range from simple /1/ to highly sophisticated /2/. Prediction power is however limited by the absence of precise measurements on the initial (primary) ionization which is Poisson-distributed. Better mean-values for a broader range of gases would be appreciated.

Another critical point is the treatment of production and multiple scattering of energetic primaries (kinetic energy above, say, 40 KeV), since those create unwelcome tails in residual- and energy loss distributions and are readily trapped and elongated in ionization by magnetic fields. As an example I show in fig.1 the high-resolution measurement of transverse charge deposit in the beginning ($1X_o$) of an electromagnetic shower, with and without a transverse magnetic field of 1.2 T, where one is interested in the deformations from magnetic trapping on a level of 1 in 1000 or so. At the same time the plot demonstrates the capabilities of gas detection in high-granularity shower measurements/3/.

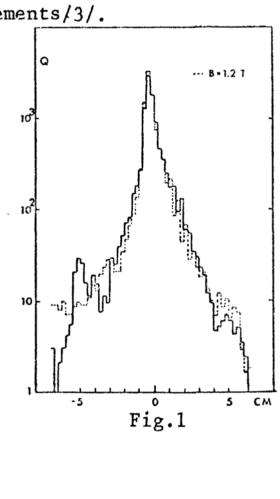

Fig.1

Electron Collection

One of the strongest points of gaseous detection is the literally infinite variety of electric field configurations that are available for electron collection onto the amplifying anode wires. In fig.2 I present a small zoology of drift schemes. Historically, the parallel-plate geometry of the multiwire proportional chamber evolved quickly into the open-cell geometry of anode- and field wires mostly used in large-volume drift chambers. More recently, the cathode-less drift chambers received quite some attention. Here, the drift field is "self-established" by positive-ion deposition on insulating or highly resistive surfaces. Highly daring geometries (fig.2) have been tried. Of course, the stability of operation in accelerator environments is rather precarious and relaxation times can range from minutes to infinity. More research in highly resistive materials (with precise and reproducible resistance) would enable rather incredible detector geometries. Other "limiting" techniques shown in fig.2 are the HPC narrow-drift channel /4/ of 8 mm width and more than 50 cm length, and the drift gap of the RICH detector where single photo-electrons drift between quartz windows over distances of more than a meter /5/.

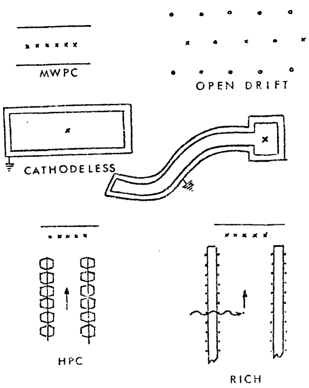

Fig.2

The boundary conditions on the drift volume, especially the action of insulators and their chargeing-up behaviour, are not too well understood and would need further study (see also the end of this race).

The superposition of a magnetic field with the electric collection field causes deviations in the drift direction ("drift angle") and changes the diffusion constant, both as a strong function of the mean free path of electrons in the gas. Notwithstanding the principal possibility to calculate these effects precisely (and to predict, for instance, the eventual deterioration of space resolution in a given field configuration), the scarce availability of basic gas parameters (like mean free path) still may lead to unpleasant surprises.

In general, parameters like transverse and longitudinal diffusion coefficients and drift velocities would be needed over a wide range of E/p values and for a large variety of detector gases. Most limiting techniques ask for limiting values also in these quantities, as for instance "unphysical" combinations like large drift velocity and, at the same time, low diffusion. Here, modern experimental techniques would offer excellent possibilities, as for instance in the recent measurements /6/ using single-electron production and detection.

Electron capture by electronegative gases and more generally negative-ion formation (especially at sizeable E/p values close to the anode wires) is another limiting effect which is probably at the origin of the observed deposit formation on the anodes. This leads to changes in wire radius and as a consequence to chamber inefficiency. Radius changes in the order of 1 micron per 10^{17} charges per cm wire length have been observed in several experiments using different gases (fig.3). With a gas amplification of 10^5, this corresponds to 10^{10} particles per cm detector gap or to only about 2 years of operation at a high-luminosity collider like the CERN-ISR. The gas plays a rather important role since in some cases the deposit could be washed off easily, whereas in some other cases silicon was found on the wires and rewiring was necessary.

Fig.3

Gas Amplification by Avalanche Formation

The detector physicist who wants to predict the response of his device instead of using word-of-mouth or cooking receipts, is faced with a deep lack of knowledge on avalanche formation. Precise values for Townsend coefficients as function of E/p (over the full range from 1 to several hundred V/cm torr) and for a large variety of detector gases are not available. The geometrical extension and development of avalanches, e.g. for different anode wire diameters, has only been superficially studied. Limitations on avalanche growth from space-charge saturation set in relatively early, at amplifications of 10^3. They are responsible for complicated time- and angle dependencies of pulse height which tend to prohibit precise charge measurements (dE/dx). Again, detector application often requests "unphysical" combinations like energy-loss measurement and coordinate measurement by charge division on the same sense wire. On the other hand, modern techniques allow precision measurements on single avalanches /6/ and do not require large experimental effort.

Finally, light emission from avalanches plays an important rôle in breakdown phenomena by photon propagation and electron extraction, especially in closed parallel-plate geometries with flat cathodes. It also causes unwanted backgrounds in the detection of single electrons (RICH technique), where photon propagation has to be counteracted by shielding walls close to the anode wires. Its use for particle detection - also rather widely proposed and studied - is not yet established in high-energy physics.

Positive-Ion Movement and Pulse Formation

The bulk of the electronic signal that can be picked off the anode or cathode structures is due to the movement of the positive ions left behind in the avalanche formation. The time dependence of this induced charge is a function of the ion drift velocity. For most applications, one is primarily interested in the first few hundred nanoseconds of this pulse, a time during which the ions move still in the radial field of the anode wire.

Experimental values on ionic drift velocity are again rather scarce in the literature, in particular in the region of very high electric field near the anode surface. In addition, rather complicated exchange processes between different species of positive ions (even in one gas, say Argon) take place at different values of electric field.

One may say that the case is saved by the fact that (in a radial field) the relative pulse shape behaves like 1/t as long as the drift velocity can be described by a power-law dependence on the electric field. This is of course nearly always fulfilled by a smooth function over a limited range of E/p. This 1/t behaviour of the avalanche signal causes a response-asymmetry (see e.g. fid.1) and influences in particular the build-up of signals from the overlap of many avalanches at different times. Complex pulse-shaping and filteringcircuitry has been employed to remove this effect. The task becomes highly non-trivial when charge measurements over long time intervals have to be made and base-line stability becomes of primary importance. Here one has to remember that in many applications the collection time is of order tens of microseconds.

In addition, most detector arrangements offer rather poor transmission-line characteristics for the extraction of fast signals. Proper termination and the avoidance of ringing can present a problem.

Up to this point one can say that the response of gaseous detectors can be described in a precise and quantitative way, with the proviso that - as explained above - basic input data are scarce in many cases. Rather complete simulation to quite a degree of detail is nevertheless possible and can be a great help in the study and design of new detectors. Especially in the development of limiting devices it can help to avoid wrong directions and the loss of time and effort in test beams. This approach has been tried as far back as a decade ago /7/. It now seems to become a common and indispensable tool in the study of gaseous detectors /8/.

Ion Migration

We are now entering a sector of the basic detection process which the detector physicist would prefer to dispense with altogether, if possible. The positive ions which have been so useful in pulse formation near the anode wire, do not want to leave the detector volume fast enough. Their very slow migration in the low electric drift field creates an effective charge accumulation such that - even at relatively modest irradiation intensities - the resulting space charge density is sufficient to influence the drift path of the ionization electrons. This results in track distortions in long-drift detectors like imaging chambers. As a consequence, the input radiation level has to be strictly limited, or the drift zone shielded from the amplification volume by a very effective gating plane such that only electrons from the few "interesting" events are allowed to reach the anode wires for amplification. This dynamic gating is a formidable problem in the immediate neighbourhood of ultrasensitive, fast electronics. In the presence of strong magnetic fields parallel to the drift field, this gating becomes even more difficult since the electrons tend to lock onto the magnetic field direction and cannot easily be deviated towards the gate wires. Using the large difference in mean free path between electrons and ions, however, the problem could eventually find a surprising solution /9/: One can imagine a "diode" gating grid at constant voltage that does not attract the electrons yet but collects (and eliminates) quantitatively the positive ions.

Ion Arrival at the Detector Boundary

This last step of the detection cycle presents problems under practically any circumstance.

If the detector boundary is insulating, the positive ions will - upon arrival - build up a surface charge. This charge is time- and intensity dependent and will modify the electric drift field near the boundary. This will entail charge losses and inefficiencies. The relaxation-time for such a process is shown in fig.4 /10, submitted to this conference/ for a typical electrode-less drift chamber when subjected to a large step in irradiation density. Similar effects are present in chambers with partially insulating cathodes (e.g. printed circuit boards). They can be minimized by carefully symmetrizing the drift potential on both sides of the boards such that no field lines end up in the insulator.

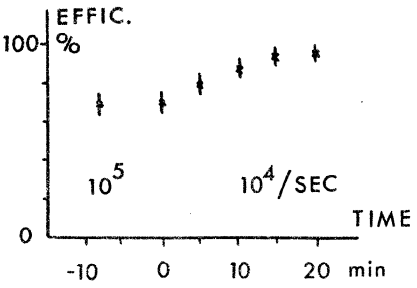

Fig.4

If on the other hand the boundary is completely conductive, the arriving ions will neutralize allright - but there is, for almost all kinds of detector gases, the tendency to polymerize upon arrival under formation of a thin insulating surface layer.This process - although, I believe, not completely understood - is well known to induce self-stable discharges and breakdown. Almost any large detector has seen its consequences in form of the appearance of sizeable dark currents followed by the growth of "whiskers" between anode and cathode and subsequent death of the chambers. A rather epic report on this can be found in /11, submitted to this conference/.

This is a good example of a limitation which has been known for generations. The "classical" remedies to it - adding small percentages of alcohol or methylal vapours - were indeed soon rediscovered /12/. Water vapour /11/ seems also to show beneficial action. If not excluded for other reasons (drift velocity, oxygen sensitivity, stability of operation), Argon with as little as possible of CO_2 seems to be the safest gas in this respect. The temerity with which large new detector systems using "dangerous" gases like Isobutane in large quantities, without protective agents, are proposed in particular for operation in limited streamer mode, is rather astonishing. A contribution to this conference /13/ shows that such high-intensity operation is indeed possible - with the addition of the proper amount of methylal.

SECOND RACE: Through the World of Large-Scale Gaseous Detectors

The modern "standard" experiment for operation at high-energy colliders has a few principal features:
- it is very large
- it is of cylindrical symmetry
- the packing of subsequent detector-layers is extremely dense
- it has a strong, in most cases solenoidal magnetic field over most of the detector volume.

Despite some heroic efforts in the past, these basic boundary conditions seem to be almost unavoidable, much to the regret of the detector designer whose choice of parameters is thus narrowed down considerably.

The detector components also tend to be arranged in a standard pattern. A high-precision vertex detector close to the interaction point is followed by a large, principal track detector, eventually by an identification stage (e.g. Cerenkov counter) and an electromagnetic calorimeter which is nowadays often placed inside the magnetic field in order to avoid disturbance from the magnet coil. A full-solid-angle hadron calorimeter which often uses the return-flux iron as converter, and muon detection close the detector assembly.

Vertex Detectors

The use of vertex detectors originated from the necessity of very precise vertex and in particular secondary vertex determination and from the experience that the space resolution of the largevolume tracking chambers cannot be made good enough due to a number of systematic limitations. For the vertex detectors, a resolution of 100 micron and below is aimed at. To achieve this, these detectors feature short wire length (not more than about 50cm), small-size drift cells (of order few mm drift path) and high gas gain to reduce electronics-induced fluctuations. Wire-geometries (fig.5) range from open-cell drift volumes to arrays of proportional tubes. Tricky field-wire geometries are used in order to reduce the large electrostatic forces encountered in small wire cells.

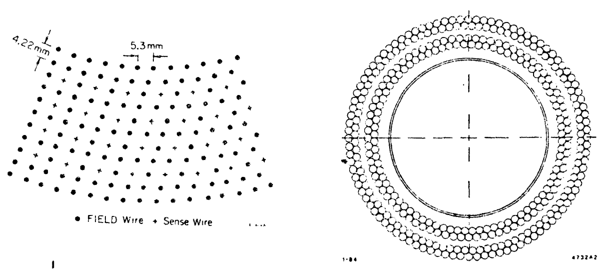

Fig.5

Another interesting feature is the extensive use of detector simulation (see also the discussion in the first race) in particular at SLAC / 8 /, in order to optimize geometry,working point and space resolution. Resolutions of order 20 micron have been reached in the high-pressure "Microjet" chamber (fig.6)/ 8 /.

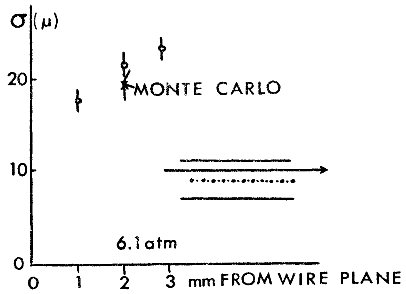

Fig.6

Another limiting approach is the time-expansion chamber /15/ where a complete analysis of the charge deposit along track elements is performed in order to gain on the statistical fluctuations from the ionization process. A resolution of 30 micron is expected using a highly sophisticated waveform-analysis (fig.7) of the charge induced on field- and sense wires.

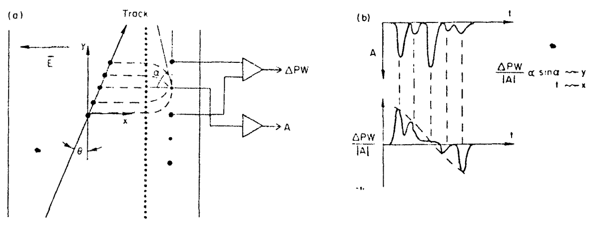

Fig.7

Large-Volume Track Detectors

Here, I can be very short since G.Viertel has described two "limiting" track detectors, the Time Projection Chamber (TPC) and the Jet Chamber in his talk at this session. The increased use of the TPC concept with its radical approach to the pattern recognition problem - although typically limited to the lower range of collider luminosity - is the result of the patient, long-range development undertaken with the Berkeley-TPC at PEP.

Jet-type chambers, which have been operated up to the highest interaction rates, are now often used with rather small drift length and a cell design that is optimized for constant drift angle in magnetic field. As an example fig.8 shows the drift cell and electron-trajectories in the MK-II detector for use at the SLAC SLC /16/.

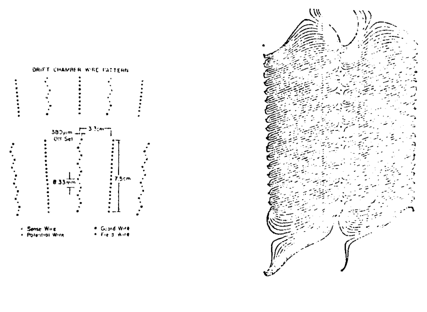

Fig.8

Particle Identification

The big event in identification techniques as well as in gaseous detection for the coming years will certainly be the large-scale application of Ring-Imaging Cerenkov detection (RICH technique). At this conference we have seen first results from a Fermilab experiment (E605)/17/ using a large, athmospheric RICH counter with He radiator and photon detection via TEA, yielding a 3 standard-deviation separation of pions and kaons at 200 GeV/c momentum.

A very large RICH counter has come into operation (fig.9) at the Omega Spectrometer /18/ at CERN. The device has more than 100 m^3 gas volume and about 10 m^2 photon detector surface.

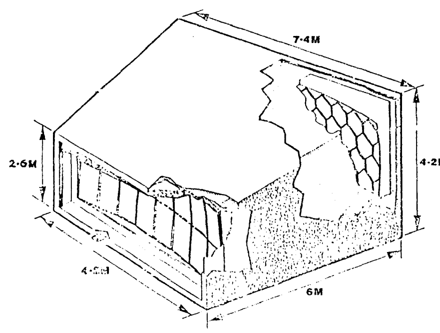

FIG 1 GENERAL VIEW OF THE RICH DETECTOR

Fig.9

Ring images for 100 GeV/c pions and protons are shown in fig.10.

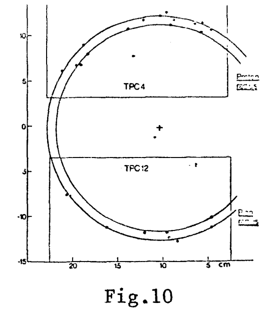

Fig.10

Another large RICH counter is going to be used in the UA2 experiment at the CERN Collider. Finally, the first attempt on complete solid-angle coverage with identification over most of the momentum range available at LEP, is being prepared for the DELPHI experiment /5/. This device will use liquid and gas radiators. Photoelectrons from both radiators will be converted , using TMAE, in a single drift tube and the photoelectrons drifted over 170 cm onto pick-up proportional chambers (fig.11).

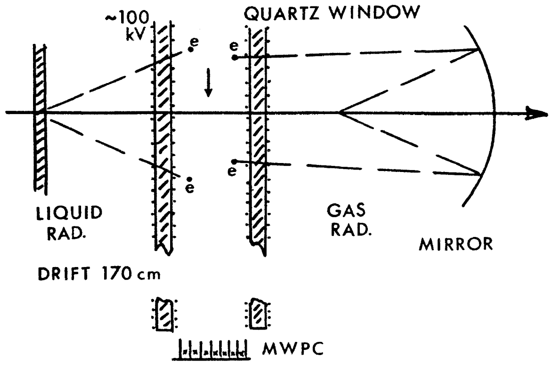

Fig.11

Most of the limiting detection principles discussed above will be combined in this one device and its realization will mark a major achievement in modern detector physics.

Calorimetry

In the detector applications discussed up to now, gas was the almost uncontested,ideal detector medium. The situation is different in calorimetry. Here, a fierce competition exists between a sizeable number of different methods and media,and gaseous detection is only one of many alternatives.

A first problem is given by the - in this context - negligible density of gases which leaves sampling-calorimetry as only application. Total-absorption calorimeters have however always played an important rôle in electromagnetic shower detection. They see at present an important come-back with the availability of new types of heavy crystals coupled to photodiode readout /19/.

Even in sampling calorimetry, gaseous detection has the drawback of rather low mean density since the detecting gas layer cannot be made arbitrarily thin. In practice however, this makes only a very small difference in detector depth if compared to denser media like plastic scintillators or liquid argon.

Gas sampling calorimeters have also had a rather bad reputation in terms of energy resolution especially for electromagnetic showers. In this respect it has been shown by many recent detector developments that - given a proper detector layout - the difference to other detection media is again very small for all practical purposes (The big step occuring in the transition from total-absorption to shower sampling).

It is in all applications that ask for shower "imaging", for good pattern recognition capability in complex events, for high granularity coordinate and angle measurements, for efficient separation of leptons from hadrons, for multishower-separation that gas detection is attractive also in calorimetry.

A "limiting" approach in this sense is the High-Density Projection Chamber (HPC) which can be seen as a TPC equipped with absorber walls inside the drift volume. An example of this new concept has been described in Dr. Viertel's talk and I will not come back to it here.

The real great domain of gas calorimeters is for the time being hadron calorimetry. Here, the use of large-surface wire-tube detectors made of extruded plastics, of brass, aluminum etc., is extremely widespread /20/. The tubes are usually operated in a limited streamer mode i.e. at very large gas amplification. This yields large, "standard" output signals which can be easily treated electronically. Pad-readout on the cathode surface for three-dimensional charge determination is easily possible in a very elegant way through highly resistive cathode surfaces. Real factories for the production of such tube arrays are being set up in order to satisfy the enormous needs in detector surface for modern large-size experiments.

REFERENCES

/1/ Nucl.Instr.Meth. 156 (1978) 81
/2/ Allison and Cobb Ann.Rev.Nucl.Sci 30 (1980) 253
Lapique and Piuz Nucl.Instr.Meth. 175 (1980) 297
/3/ DELPHI/HPC group private communication
/4/ Fischer proc.Novosibirsk Conf. Coll.Instr. (1984)
/5/ DELPHI Techn.Rep. CERN LEPC 83-3 (1983)
/6/ Piuz Nucl.Instr.Meth. 205 (1983) 425
/7/ Proc. Intern. Meeting Prop. and Drift Ch. Dubna (1975) p.152
/8/ Va'vra Nucl.Instr.Meth. 217 (1983) 322
SLAC-PUB-3131 (1983)
see also Piuz /2/
/9/ Amendolia et al CERN/EF 84-11
J.Augustin (DELPHI Coll.) private commun.
/10/ Budagov et al Contr. 120 this Conference
/11/ Tasso Vertex Detector Contr. 645 this Conf.
/12/ Charpak et al Nucl.Instr.Meth. 99 (1972) 279
/13/ Alekseev et al Contr. 119 this Conference
/15/ Walenta et al Proc. SLAC Conf.Coll.Instr. (1982)
/16/ Hanson Proc. Novosibirsk Conf.Coll.Instr. (1984)
/17/ Contr. to this Conference
/18/ P.Sharp (WA69 expt) Private Communication
/19/ Proc. Novosibirsk Conf.Coll.Instr. (1984)
/20/ Iarocci Proc. SLAC Conf.Coll.Instr. (1982)

A RING IMAGING WATER CERENKOV COUNTER FOR ν_μ-e SCATTERING

Presented by A. Staude
University of Munich, FRG
Ecole Polytechnique-Munich-Saclay-Collaboration

Scattering of muon neutrinos on electrons is a purely leptonic process, free of theoretical uncertainties and is well suited for a precision measurement of the weak mixing angle . The ratio of the cross-section for ν_μ and $\bar{\nu}_\mu$ scattering is very sensitive to $\sin^2\theta_W$: A change of $\sin^2\theta_W$ by 0.005 at $\sin^2\theta_W = 0.21$ changes the total cross-section ratio by about 4%.

The most characteristic feature of ν_μ-e scattering is the small angle of the electron with respect to the neutrino direction. From the kinematical relation $1-y=E_e\theta^2_e/2m_e$ ($y=E_e/E_\nu$), $\theta_e < 32$ mrad/$\sqrt{E_e}$(GeV). The most serious background is neutrino-nucleon scattering, which has a much wider angular distribution of the emitted particles but a $\sim 10^4$ times higher cross-section and is usually subtracted by an extrapolation in $E_e\theta^2_e$.

For a reliable background subtraction, a detector must have good angular resolution and particle identification for forward particles. A possible detector [1] uses Cerenkov light from a water radiator which also serves as target. The light is detected in three different arrays of phototubes: a) A ring imaging counter which detects light from forward particles; b) A "shower scanner", which is sensitive to light emitted by particles within 100 mrad around the beam direction; c) An "inner detector" for the measurement of the total reaction energy. The phototubes of this detector are arranged on a regular grid and sample the total emitted Cerenkov light.

Detectors a) and b) have been tested with a prototype set-up consisting of a 4.4 m long tank of 1 x 1.5 m² cross-section, filled with purified water and exposed to a beam inclined by 40 mrad upwards to simulate the CERN neutrino beam. Cerenkov light from forward particles traverses the water surface close to the angle of total reflection and is focused by a spherical mirror (R=12m) on an array of photomultipliers. The image is an arc of a circle, whose position depends only on the angle of the particle. The image moves vertically by $\sim$ 2.5 cm for a change of the vertical particle direction of 1 mrad. Fig. 1 shows light distributions versus the vertical angle, averaged over the azimuthal angular range of ± 100 mrad, for a muon, a 15 GeV electron and a 15 GeV pion. The distributions show a peak at zero angle but differ significantly due to the different interactions in water. The peak position for electrons is measured with a FWHM resolution of 14 mrad/$\sqrt{E_e}$(GeV) in the range 3-20 GeV. The resolution is, however, not gaussian: The fraction of events outside 2σ decreases from 33% (at 3 GeV) to 10% (at 20 GeV).

Pions also give much less light than electrons (which give 47 Photoelectron/GeV) in the focal plane. Both criteria combined give a π rejection of 5×10^{-3} and even better for muons.

Forward single γ's are indistinguishable from e's in the focal plane. They are suppressed with the shower scanner which views the event in slices of 1/3 radiation lengths along the beam direction. In the first slices, γ's yield about twice as much light. The allows to suppress γ's by a factor 5, keeping 80% of the electrons.

Monte-Carlo calculations using the results of this test, and assuming a knowledge of the relative $\nu/\bar{\nu}$ flux to 4%, show that a precision of $\Delta\sin^2\theta_W=0.005$ can be obtained in a realistic experiment. Given a precise knowledge of the Z^0 mass, this would test the standard model beyond the Born terms; corrections to these would be measured to 25% of their value.

[1] L. Behr et al., CERN/SPSC/P199 (1984).

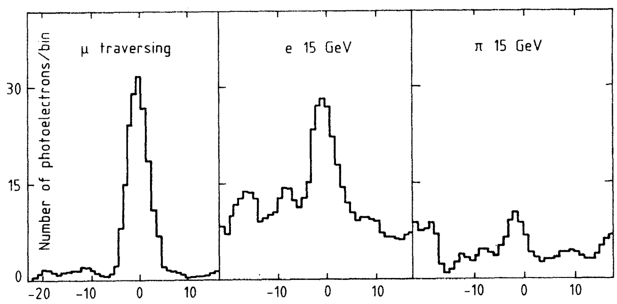

FIG. 1 : VERTICAL ANGLE (mrad)